Fuel 212 (2018) 240–255

Contents lists available at ScienceDirect

Fuel

journal homepage: www.elsevier.com/locate/fuel

Full Length Article

A method for retrieving char oxidation kinetic data from reacting particle trajectories in a novel test facility

Wojciech P. Adamczyk[a], Ryszard A. Białecki[a], Mario Ditaranto[b], Nils Erland L. Haugen[b], Anna Katelbach-Woźniak[a], Adam Klimanek[a,*], Sławomir Sładek[a], Andrzej Szlęk[a], Gabriel Węcel[a]

[a] Institute of Thermal Technology, Silesian University of Technology, Konarskiego 22, 44-100 Gliwice, Poland
[b] SINTEF Energi A.S., Sem Saelands vei 11, 7034 Trondheim, Norway

GRAPHICAL ABSTRACT

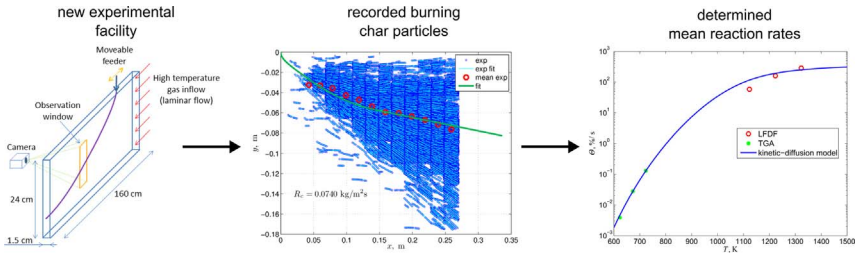

ARTICLE INFO

Keywords:
Coal combustion kinetics
Combustion rates
Cion
Kinetic data
Inverse method
Uncertainty quantification

ABSTRACT

In this paper, a new method for retrieving char combustion rates is presented. The method is based on an observation that the curvature of a trajectory of a freely falling and reacting char particle in a horizontal laminar flow changes due to the change of the particles mass. An experimental facility was designed and built allowing for recording reacting particle trajectories and determining oxidation kinetics. A brief description of the experimental facility and measurement procedure is given. In this procedure, a model of a freely falling particle in a laminar horizontal flow was developed. The model comprises a set of ordinary differential equations that predict a particle trajectory for given rate constants. The trajectory predicted by the model is then fitted to the measured trajectories by changing the rate constants. The best fit corresponds to the mean rate constant. Moreover, measurement results for Janina coal char combustion in air at various temperatures are presented. The key input parameters of the model are identified by a global sensitivity analysis, and the uncertainty in the results is quantified. The method is validated by comparison with TGA results obtained from the literature. Finally, the experimental data are used to determine rate coefficients of a kinetic-diffusion surface combustion model. The presented methodology is suitable to determine the kinetic data, however its further development is required in order to improve the accuracy of the measurements and include the more complex physico-chemical processes that occur during carbon conversion.

1. Introduction

Improvement of existing combustion chambers and development of new combustion techniques requires understanding of the elementary processes occurring during fuel conversion. The understanding should be accompanied by reliable data that can be used to predict the system behavior at various conversion stages. In recent years, numerical modeling of combustion processes by means of computational fluid

* Corresponding author.
E-mail address: adam.klimanek@polsl.pl (A. Klimanek).

http://dx.doi.org/10.1016/j.fuel.2017.10.020
Received 20 March 2017; Received in revised form 17 June 2017; Accepted 5 October 2017

Nomenclature

Nomenclature

A	area (m^2); pre-exponential factor ($s\ m^{-1}$)
C	diffusion rate constant ($s\ K^{-0.75}$)
C_d	drag coefficient (−)
d	diameter (m)
D	diffusion coefficient ($m^2\ s^{-1}$)
E	activation energy ($J\ kmols^{-1}$)
g	acceleration due to gravity ($m\ s^{-2}$)
Gr	Grashof number (−)
m	mass (kg)
$\dot{m}$	mass flow rate ($g\ s^{-1}$)
M	molecular weight ($kg\ kmol^{-1}$)
p	pressure (Pa)
R	universal gas constant, $R = 8314.46\ (J\ kmol^{-1}K^{-1})$
R_c	mean reaction rate constant ($kg\ m^{-2}\ s^{-1}$)
R_{dif}	diffusion rate ($m\ s^{-1}$)
R_{kin}	kinetic rate ($m\ s^{-1}$)
Re	Reynolds number (−)
Ri	Richardson number (−)
Sc	Schmidt number (−)
Sh	Sherwood number (−)
t	time (s)
T	temperature (K) or (°C)
u	horizontal velocity component ($m\ s^{-1}$)
v	vertical velocity component ($m\ s^{-1}$)
x	horizontal spacial coordinate (m)
y	vertical spacial coordinate (m)

Greek symbols

ϕ	sphericity (−)
μ	mean (units vary); dynamic viscosity ($kg\ m^{-1}\ s^{-1}$)
ν	kinematic viscosity ($m^2\ s^{-1}$)
ρ	density ($kg\ m^{-3}$)
σ	standard deviation (units vary)
Θ	normalized char conversion rate (s^{-1})
ω	weight (−)

Super- and subscripts

0	initial
p	particle
s	slip; sphere
t	terminal; total

dynamics (CFD) tools became an integral part of the design and optimization processes. The models used in the simulations require closure approximations, which are based on experimental data. In order to improve the predicted system behavior, the quality of the data should be high and the closure models themselves should be fast, robust and accurate. Kinetic parameters of drying, devolatilization and char gasification/combustion, together with ignition characteristics, are crucial elements of simulations of combustion processes. It should be stressed that the experimental data, from which the kinetic parameters are obtained, should be determined at relevant process conditions. Specifically the temperature, the heating rate, the thermal history, the pressure and the atmosphere are of importance [1,2]. Drop tube furnaces (DTF) are already standard devices used to retrieve such data. In recent years, many studies were devoted to characterization of solid fuels. These include ignition characteristics [3–7], kinetic parameters of devolatilization [1,2,8,9], combustion [10–13] and gasification [14–18] processes. The conditions achievable in drop tube reactors are close to or are the same as those observed in the real pulverized coal systems. The investment and operating costs of a DTF are however relatively high and the measurement procedures are time consuming. Another method that is frequently used to obtain kinetic data is the Thermogravimetric analysis (TGA). It is however restricted to low heating rates and lower temperatures (below 1000 °C) due to the inability of observing the real diffusion restrictions at high temperatures. At lower temperatures combustion and gasification rates are controlled by chemical reactions at the solid fuel particle surface. Therefore, TGA is frequently used in combination with a DTF to determine fuel characteristics at low and high temperature limits [15,16].

In this paper, a new method of retrieving char combustion rates is presented. The method is based on the fact that the trajectory of a freely falling and reacting char particle in a horizontal laminar flow changes due to change of particle mass. An experimental facility, a laminar flow drop furnace (LFDF), was designed and built at the Institute of Thermal Technology, Gliwice, Poland that implements the idea. The experimental facility, as well as basic concepts of the new method, have already been introduced in a previous study [19,20]. In the present work, the method is presented in detail and results of determination of char combustion rate in air are described. A global sensitivity analysis (SA) and uncertainty quantification (UQ) are then conducted to determine the most influential parameters in the model and to quantify uncertainty in the retrieved particle density and mean reaction rate constants. The obtained results are then compared with TGA data adopted from the literature, which were conducted for the same coal and atmosphere. Finally, the experimental data are used to fit a kinetic-diffusion surface combustion model.

2. The experimental facility

The concept of the experimental facility [19,20] is based on an observation that the curvature of the trajectory of a freely falling particle in a horizontal flow changes due to changes of the particle's mass. This behavior can be visualized by comparing trajectories of burning

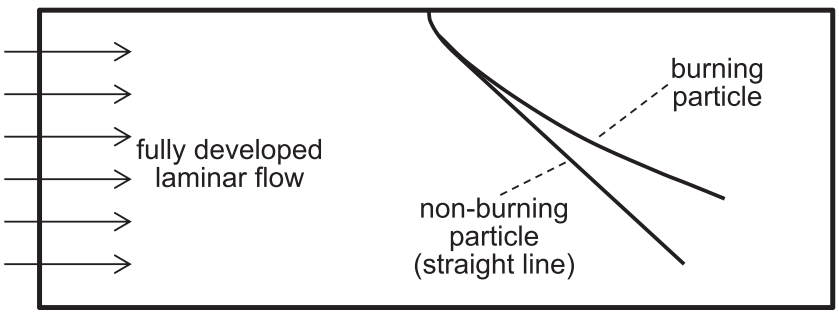

Fig. 1. Behavior of non-reactive and reactive particle falling in laminar flow field.

and non-burning char particles introduced to a laminar horizontal flow, as shown in Fig. 1. The trajectory of a burning particle deviates from the trajectory of constant-mass particle due to its mass loss. It is anticipated that the change of particle trajectory can be used to determine the mass loss of the reacting particle. This can be achieved by recording reacting particles' trajectories by means of a high-speed camera and retrieving their mass changes by virtue of inverse analysis. These postulates were verified using the designed and built experimental laboratory scale laminar flow drop furnace (LFDF). The furnace is a rectangular channel in which hot gas flows horizontally and the particles are introduced through fuel injection ports at the top wall of the channel. A schematic view of the furnace is presented in Fig. 2, where the dimensions of the channel are shown as well. The walls of the furnace are built out of quartz slabs and are separated by a 1.5 cm gap. The quartz slabs are surrounded by electric heaters and insulation, allowing a constant temperature to be maintained in the furnace. Particles are recorded using a CMOS camera situated in front of a vertical observation window. During the experiment, the fuel feeding system can be moved and the pulverized char particles can be supplied from various injection ports. At the same time the camera can move in the vertical direction. Therefore a large portion of the furnace space can be observed and particles' trajectories can be recorded. The gas can be heated up to 1100 °C. The gas flow is controlled by two mass flow meters for preparing oxidizers of desired compositions. The applied fuel feeder facilitates a controlled fuel supply. A typical char mass flow rate to gas mass flow rate is $\sim 10^{-4}$, which allows for combustion of individual particles in an undisturbed flow. The length of the channel is selected such that a fully developed laminar flow is obtained at the char injection region. For further information on the experimental facility and measurement procedures, the reader is directed to our previous papers [19,20].

2.1. Constraints on flow and char particles

The fluid flow in the test facility must be maintained laminar to preserve a steady and known gas velocity profile in the test section. Furthermore, particle properties must be kept within certain ranges in order to be able to observe the departure from linear particle trajectory, when the particle loses mass due to combustion. Taking the critical Reynolds number Re = 1400 [21] as for infinite parallel plates, above which the flow becomes turbulent, one can obtain the mean and maximum (in the center) gas velocities in the chamber at given temperature and gas composition. If the angle between particle trajectory and horizontal gas velocity component is taken as approximately 45°, the departure from the linear trajectory due to combustion can be observed. This condition is satisfied if the particle terminal velocity equals the gas velocity in the center of the chamber. These conditions allow for determining the maximum particle diameters (for a given particle density) that can be used in the experiments. In Table 1 the critical (corresponding to Re = 1400) mean and maximum (in the center of the channel, $u_{max} = 3/2 u_{mean}$) gas velocities are presented along with the corresponding particle diameters. The results were obtained for air and oxy-fuel conditions (O_2/CO_2 = 3/7 vol.) and for selected gas temperatures and particle densities. The minimum gas temperature was selected to be 900 °C due to the fact, that very little departure from the linear trajectory was observed in our previous experiments for lower temperatures. The temperature of 1100 °C is the current maximum temperature that can be reached in the test facility. As can be observed very large maximum particle diameters can be theoretically examined in the test facility, however in practice the sizes should be smaller in order to observe complete burnout of the particles. The current height of the channel is 24 cm, which allowed to observe complete burnout of particles smaller than 140 μm and of densities of approximately 1100 kg m^{-3}. As will be discussed in Section 3.1.1 the buoyancy effects can become significant if the particles diameter and/or density become sufficiently small, which limits the use of the facility for fine and less dense particles if the buoyancy effects are not included in the analysis. It can be summarized that the flow conditions and particles that can be examined in similar facilities of this type will depend on the dimensions of the channel, the maximum temperatures that can be reached in the system and oxidizer composition. Important role is played by the coal/char properties, specifically its diameter and density as well as its the time of combustion.

2.2. Fuel

In all experiments conducted in this study a coal char produced from a bituminous coal was used. The coal was extracted from a Polish coal mine Janina, whose reserves are the largest of all the existing coal mines in Poland. The char was produced from a milled coal in nitrogen atmosphere with a slow-heating rate (5 K/min) up to a final temperature of 1000 °C and was kept at the final temperature for 30 min. Thus, a dense and low reactivity char was produced. The obtained char was then sieved to obtain a desired size fraction. The proximate and ultimate analyses of the Janina coal is presented in Table 2.

3. Retrieving the combustion rate

During the experiment, the particles' trajectories are recorded using the camera, while an in–house image processing tool retrieves the particles positions in time. At each camera position, a number of particles are recorded. Although the char particles are carefully prepared and sieved to obtain a narrow size distribution, their shapes, diameters as well as their composition varies, influencing their trajectories. Since the combustion rate should represent a mean reaction rate, representative of the whole sample, a mean trajectory representing the whole sample is also desired. This mean trajectory is represented by a few discrete points (mean particle positions) obtained by averaging the recorded trajectories. The averaging is realized for particles released from a single injection port, i.e. a single feeder position. An example of recorded char particles in nitrogen at 1000 °C is presented in Fig. 3. The particles were released from 7 injection ports and the recorded trajectories were used to calculate the mean particle positions, representing the mean trajectory of the whole fuel sample.

Therefore, the final data representing the mean trajectory comprises a set of a few discrete points. An inverse analysis can then be applied to adjust a trajectory predicted by a model to the discrete, experimentally

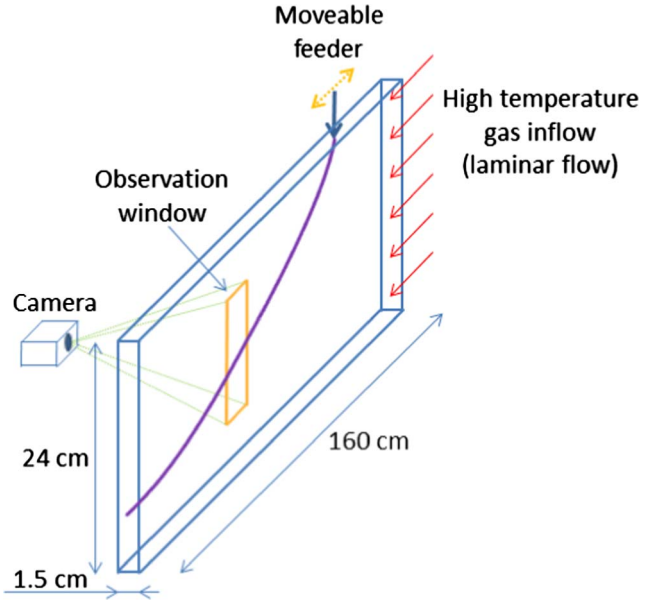

Fig. 2. Idea of the measurements and dimensions of the experimental facility.

Table 1
Limiting conditions of the facility.

	air		O_2/CO_2 = 3/7	
T (°C)	900	1100	900	1100
u_{mean} (m s^{-1})	14.8	19.2	10.6	13.8
u_{max} (m s^{-1})	22.2	28.8	15.9	20.7
ρ_p (kg m^{-3})	d_p (mm)			
600	8.7	11.8	6.7	9.0
900	6.2	8.4	4.9	6.5
1200	5.0	6.7	3.9	5.2

determined particle positions. For this, a model, which allows for calculating a reactive particle trajectory, has to be formulated. The model comprises the direct problem in the inverse analysis.

3.1. The direct problem

The model equations are formulated based on the forces acting on a single particle. In this study, the acceleration of the particle is attributed solely to the balance between the gravitational force and the drag. The force balance together with the definitions of the particle velocities form the equations from which $x_p(t)$ and $y_p(t)$ can be calculated. These are the equations for particle velocity in x direction

$$\frac{dx_p}{dt} = u_p \tag{1}$$

particle velocity in y direction

$$\frac{dy_p}{dt} = v_p \tag{2}$$

particle acceleration in x direction

$$\frac{du_p}{dt} = \frac{18\mu}{\rho_p d_p^2} C_d \frac{Re_p}{24}(u-u_p) \tag{3}$$

particle acceleration in y direction

$$\frac{dv_p}{dt} = \frac{18\mu}{\rho_p d_p^2} C_d \frac{Re_p}{24}(v-v_p) + \frac{g(\rho_p-\rho)}{\rho_p} \tag{4}$$

where u_p and v_p are the particle velocities in the x and y direction, respectively, ρ_p and d_p are particle density and diameter, ρ and μ are the density and dynamic viscosity of the fluid, C_d is the drag coefficient, u and v are gas velocities in x and y direction, g is the gravitational acceleration and Re_p is the particle Reynolds number defined as

$$Re_p = \frac{\rho d_p u_s}{\mu} \tag{5}$$

where u_s is the relative velocity of the fluid with respect to particle velocity; such that $u_s = |u-u_p|$ in the x direction and $u_s = |v-v_p|$ in the y direction. The drag coefficient is determined using the correlations by Haider and Levenspiel [22], which take into account the sphericity ϕ of the particles. The sphericity is defined as

$$\phi = \frac{A_s}{A_p} \tag{6}$$

where A_s is the surface area of a sphere having the same volume as the particle and A_p is the actual surface area of the particle.

At the current stage of development of the methodology, it is assumed that a mean particle conversion rate is to be determined. The rate of change of mass is assumed to be

$$\frac{dm_p}{dt} = -R_c \pi d_p^2 \tag{7}$$

where m_p is the particle mass and R_c is the mean reaction rate constant in kg m^{-2}s^{-1}. The mean reaction rate constant R_c encompasses all the complex physico-chemical processes that occur during particle conversion and thus is a drastic simplification of the reality, however for the current stage of development, it is desirable to limit the number of unknowns and to represent the conversion process by a global parameter. Such an approach allows for analysis of the parameters influencing the determination of the reaction rate.

Eq. (7) is coupled with the set of Eq. (1)–(4) by the particle density

$$\rho_p = \frac{6m_p}{\pi d_p^3} \tag{8}$$

If R_c is known, solving the above set of equations allows determining the particle trajectory ($x_p(t)$ and $y_p(t)$) for a reacting particle. The solution is subject to the following initial conditions

$$\begin{cases} x_p(0) = 0 \\ y_p(0) = 0 \\ u_p(0) = 0 \\ v_p(0) = -v_t \\ m_p(0) = \rho_{p0}\pi d_{p0}^3/6 \end{cases} \tag{9}$$

where ρ_{p0} and d_{p0} are the initial particle density and diameter, respectively and v_t is the terminal velocity, i.e., the maximum free fall velocity of the particle determined at the conditions of the flow. Justification for the terminal velocity used as the boundary condition will be presented in Section 3.1.5. It is assumed that the flow of particles is two dimensional (x,y), therefore the possible deviation of the particle's trajectory in the z direction is ignored. This is justified due to a narrow depth of field (~3 mm) of the camera that was used in the experiments. An analysis of the velocity profile variation in the channel leads to a conclusion that the particles falling within the 3 mm depth of field can be exposed to gas velocity differing at most by 4%. The algorithm used to determine the particle positions from recorded images accepts only sharp particle images, so that the particles that are not in the center of the reactor are ignored. From the experience gained so far, only a small percentage of the particles fall outside the depth of field. This allows one to assume that the observed particles flow in the gas of maximum velocity u, which is in the center of the reactor.

3.1.1. Buoyancy effects

Further assumption of this study is that the gas density ρ entering Eqs. (4) and (5) is constant for a given test and equal to the density of the free stream air. The reason of this assumption is the lack of possibility measuring the burning particle temperature. Therefore the buoyancy effects associated with the increase of gas temperature near the particle surface and the net outflow of CO and CO_2 from the particle surface are neglected at the current stage of development of the methodology. As discussed by Richter et al. [23], this assumption is justified at certain conditions only. The importance of the buoyancy

Table 2
Proximate and ultimate analyses of the Janina coal.

Proximate analysis (wt.% ar)			Ultimate analysis (wt.% db)					Higher heating value (M J kg^{-1} ar)
Moist.	Ash	Vol.	c	h	o	n	s	HHV
11.0	12.28	30.43	65.44	4.48	13.55	1.02	1.71	22.910

ar – as received; db – dry basis.

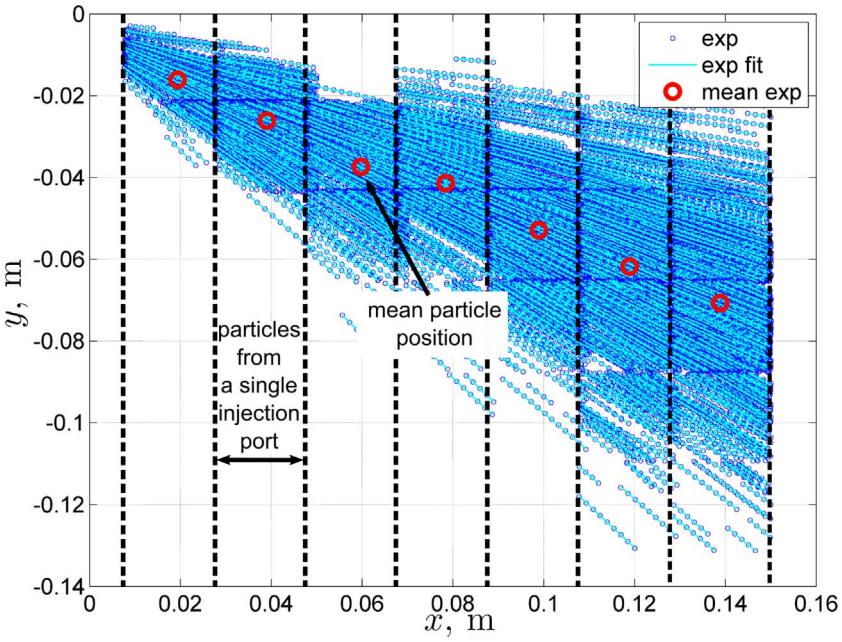

Fig. 3. Recorded trajectories and their average positions comprising the experimental data used to retrieve the char conversion.

and forced convection can be examined by estimation of the Richardson number

$$\mathrm{Ri} = \mathrm{Gr}/\mathrm{Re}_p^2 = \frac{g(\rho-\rho_s)d_p^3}{\rho_s \nu^2} \tag{10}$$

where ρ_s is the density of the fluid at the particle surface and ν is the kinematic viscosity. If the Richardson number is $\mathrm{Ri} < 0.1$ the natural convection is negligible when compared to the forced convection. Results of an analysis of the possible values of the Richardson numbers for conditions examined in this study are presented in Figs. 4 and 5, where calculated Richardson numbers for two particle diameters equal to 80 and 120 μm are presented as a function of particle temperature and density. It was assumed that the fluid at particle surface is a mixture of 50% vol. CO and 50% vol. CO_2, the free stream gas temperature was $T = 1323$ K and the particle Reynolds number was calculated for terminal velocities of the particles. As will be discussed later, the particles used in the experiments of this study were of mean initial diameter equal to 119.2 μm and density of 1076.4 kg m^{-3}. As can be seen in Fig. 4 and 5 the Richardson numbers are always smaller than 0.1 for the larger particles, while they can reach values close to 0.3 for high particle temperatures exceeding 2000 K and low particle densities. The latter conditions can occur at the end of particle burnout, where there is lower particle density and still high, though decreasing, particle temperature. Experiments in an entrained flow reactor presented in [24] indicate that char particles (d_p~ 115μm) burning in a 12% O_2 environment with a gas temperature of ~1600 K reach a temperature of ~2000 K prior to burnout, while particles burning in a 24% O_2 environment have a temperature of ~2200 K. This indicates that the particle surface temperatures can be a few hundred Kelvins higher than gas temperature. The highest air temperature in this study was 1323 K, therefore it is expected that the particle temperatures were lower than 2000 K and thus the buoyancy effects can be neglected with accepting the associated error. At the last stages of combustion, however the

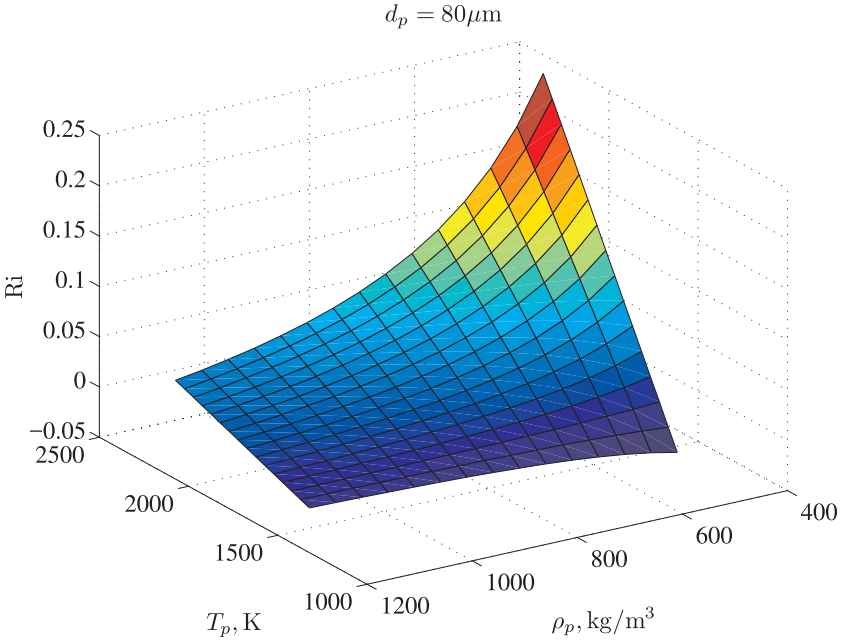

Fig. 4. Richardson number for char particles of $d_p = 80$ μm at conditions considered in this study.

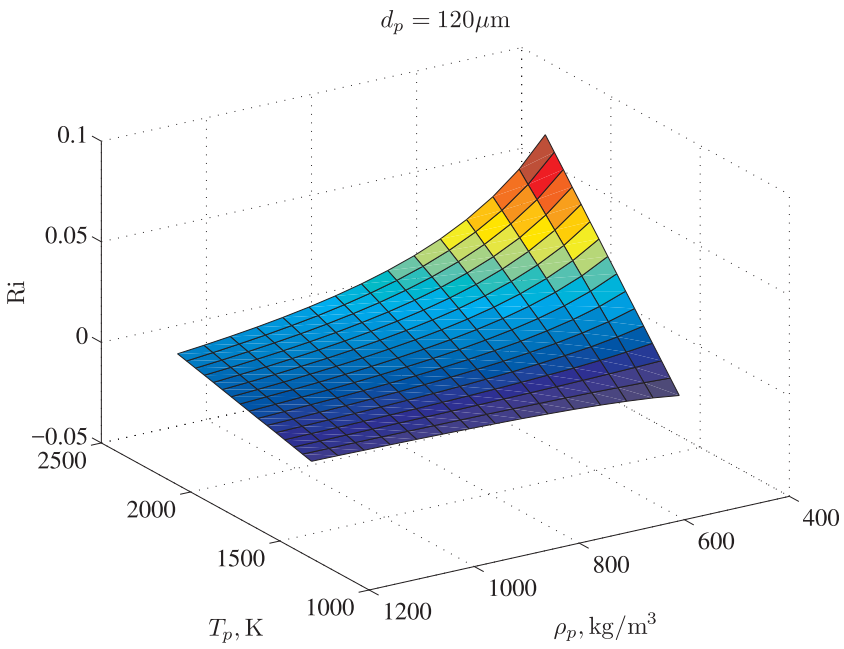

Fig. 5. Richardson number for char particles of d_p = 120 μm at conditions considered in this study.

natural convection can become important and the buoyancy effects should be included in the analysis in the future, when particle temperature measurement possibility will be available at the experimental facility.

3.1.2. The gas velocity

The vertical gas velocity v is assumed to be 0 at all times. The horizontal velocity varies in the vertical direction $u(y)$. In our previous study [19], the velocity profile $u(y)$ was determined from a finely resolved CFD simulation of the flow in the reactor performed for the same conditions (mass flow rate, temperature, gas composition) as in the experiment. In order to accelerate the computations, the analytical solution for laminar flow in a rectangular channel of Spiga and Morino [25] was used. Following Blythman et al. [26], 100 terms in the infinite sums of the analytical solution was used in the computations which produced a converged velocity field. Comparison of the $u(y)$ and $u(z)$ velocity profiles obtained from the CFD simulation and the analytical solution in the center of the rectangular channel are presented in Fig. 6. The profiles were obtained for a flow of nitrogen at 1000 °C with a mass flow rate of $\dot{m}$ = 0.224 g s^{-1}. The channel cross section has a width of 0.015 m and a height 0.24 m. The position y = 0 m corresponds to the top of the reactor were the particles are introduced. Since the velocities coincide this confirms that the analytical method and the CFD simulations were adequate. Since the computations by means of the analytical solution are much faster, the analytical solution will be used in the calculations hereafter.

3.1.3. The initial particle diameter

Along with the particle trajectories, the particle diameters were measured by means of the optical system. The procedure for calculating the particle diameters was described in our previous study [19]. The particle diameter distribution determined for the Janina coal is

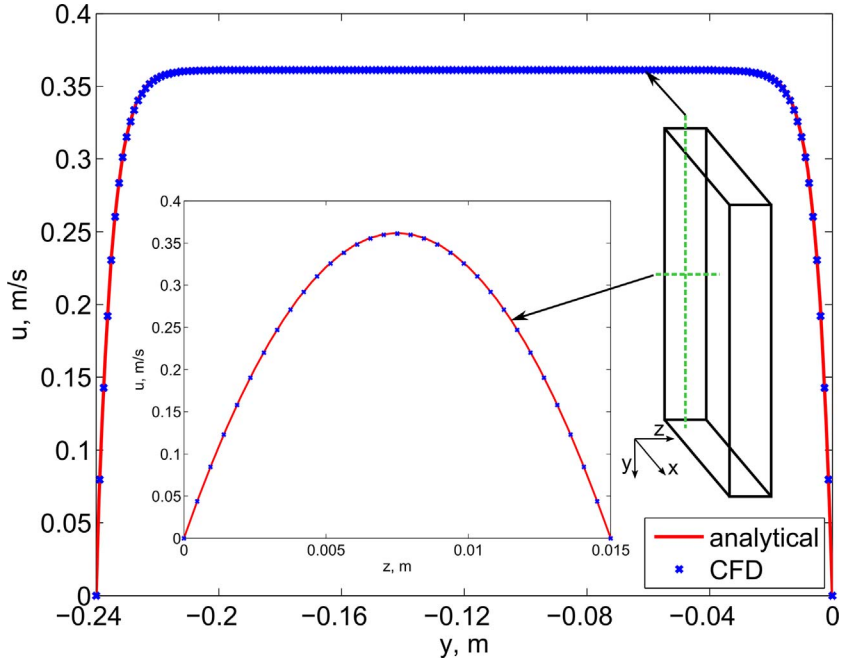

Fig. 6. Comparison of the gas velocity profiles in the center of the reactor obtained from CFD model and analytical solution of Spiga and Morino [25].

presented in Fig. 7. The normal distribution obtained for the corresponding mean particle diameter $\mu_{d_p} = 119.2\,\mu m$ and standard deviation $\sigma_{d_p} = 15.9\,\mu m$ are also presented. The mean of the measured particle diameters μ_{d_p} can be used as the initial particle diameter d_{p0} entering Eq. (9). If the particle diameter does not change during combustion, the particle diameter d_p entering Eqs. (3)–(8) remains constant and equal to d_{p0}.

3.1.4. The particle sphericity

The particle sphericity was measured together with the particle diameters using the optical system as described in our previous study [19]. The mean and standard deviation of the particle sphericity is provided in Table 3.

3.1.5. The inlet particle velocity

The vertical component of the particle velocity at the inlet of the reactor, $v_p(0)$, should correspond to the real velocity at the char feeder outlet. The inlet is however not visible in the current experimental setup. In our previous study [19], the vertical velocity at the reactor inlet was assumed to be $v_p(0) = 0$. In order to provide more reliable input data to the model, the particle velocities at the feeder outlet were measured for 289 particles. The measurements were conducted in air at room temperature. The cumulative distribution function of the determined particle velocities is presented in Fig. 8. The particle velocities were normally distributed and a normal distribution, calculated using the corresponding mean value $\mu_{v_p} = 0.2811\ m\ s^{-1}$ and standard deviation $\sigma_{v_p} = 0.0479\ m\ s^{-1}$, is also shown in the figure. Calculated terminal velocity for a particle of $d_p = 120\ \mu m$, $\rho_p = 1100\ kg\ m^{-3}$, sphericity $\phi = 0.75$ in air at 20 °C is $v_t = 0.3123\ m\ s^{-1}$. Comparing this result with the mean measured velocity, we can conclude that the velocities of the particles leaving the feeder are already close to terminal velocities and the terminal velocity can be a much better estimate of the particle velocity at the reactor inlet than the previously assumed value. Thus, hereafter we use the terminal velocities as the boundary condition for the model ($v_p(0) = -v_t$). It should be stressed here that the relatively large width of the initial velocity distribution is an effect of the distribution of the initial particle diameter and its sphericity. This influence can be recognized when Eq. (4) is examined. Assuming that the particle reaches the terminal velocity ($dv_p/dt = 0$) and neglecting the buoyancy ($\rho_p \gg \rho$), Eq. (4) reduces to a simplified formula for the terminal velocity of particle

$$v_p = \sqrt{\frac{8 m_p g}{\rho C_d \pi d_p^2}} \tag{11}$$

Applying the uncertainty propagation rule and taking into account the effect of particle diameter only, one obtains

$$\sigma_{v_p} \approx \sqrt{\left(\frac{\partial v_p}{\partial d_p}\right)^2 \sigma_{d_p}^2} = \sqrt{\frac{8 m_p g}{\pi \rho C_d}}\,\frac{1}{d_p^2}\sigma_{d_p} \tag{12}$$

The standard deviation of particle velocity (particle terminal velocity) calculated from Eq. (12) is $\sigma_{v_p} = 0.0414\ m\ s^{-1}$. Comparing this result with the standard deviation obtained from the experiment ($\sigma_{v_p} = 0.0479\ m\ s^{-1}$) we can conclude that the relatively large width of the distribution of the particle velocity is an effect mainly of the wide distribution of particle diameter.

Table 3
Mean values and standard deviations of the parameters in the experiment in nitrogen.

	d_p (μm)	v_t (m s^{-1})	ϕ (−)	$\dot{m}$ (g s^{-1})	T (K)
Mean, μ	119.2	0.1629	0.7737	0.223778	1273.15
Standard deviation, σ	15.9	0.0327	0.0580	0.000448	1.79

3.1.6. The initial particle density

The initial particle density ρ_{p0} needs to be provided in order to solve the governing equations. This density can be determined by applying an inverse analysis for a non-reactive case, where the particle mass m_p and diameter d_p remain constant. The inverse analysis will be described in the next section.

3.2. The inverse problem

The measured particle trajectories determined at each camera position (observation window) allow for determining discrete points, representing mean particle trajectory at each camera position, which are denoted as $\overline{x}_{p,i}$ and $\overline{y}_{p,i}$. This data can be used to evaluate the particle density ρ_p (non-reactive case) and mean reaction rate R_c (reactive case).

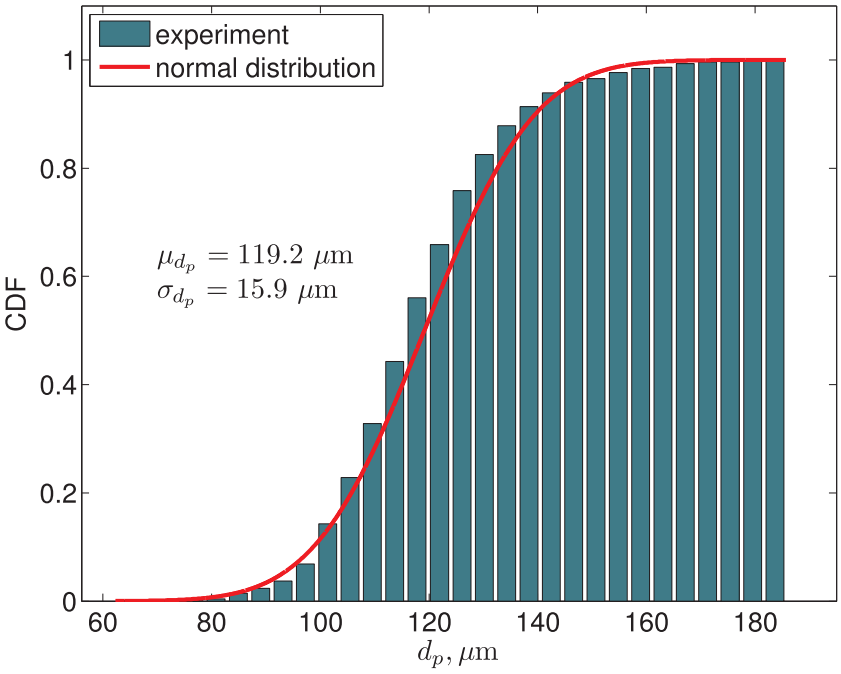

Fig. 7. Cumulative distribution function of measured particle diameter and normal distribution fit with mean value $\mu_{d_p} = 119.2\,\mu m$ and standard deviation $\sigma_{d_p} = 15.9\,\mu m$.

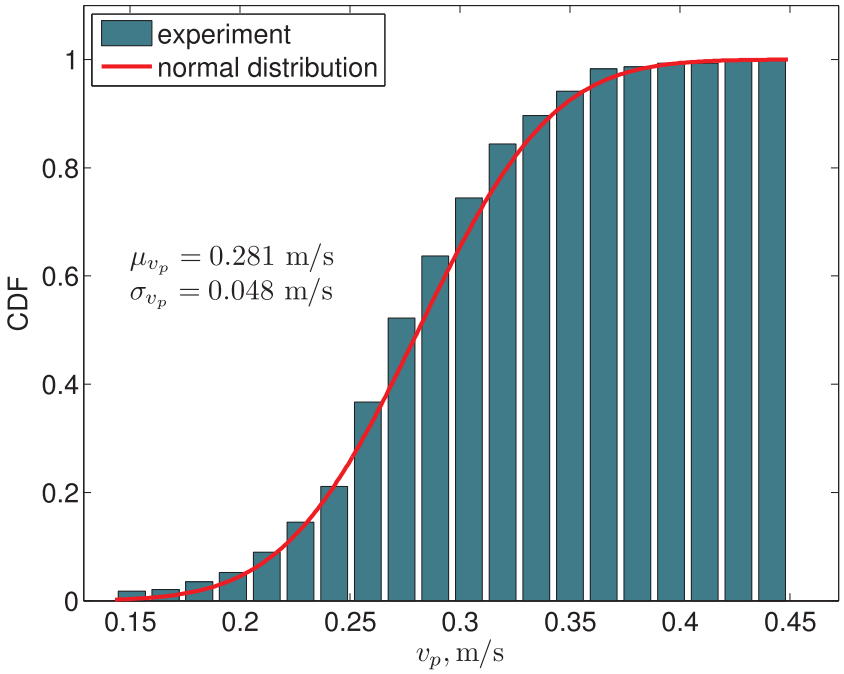

Fig. 8. Cumulative distribution function of measured particle velocities at feeder outlet and normal distribution fit with mean value $\mu_{v_p} = 0.2811\ \mathrm{m\,s^{-1}}$ and standard deviation $\sigma_{v_p} = 0.0479\ \mathrm{m\,s^{-1}}$.

3.2.1. The non-reactive case

If the particle is non-reactive or the atmosphere is inert, the mean reaction rate constant R_c will be 0 at all times and Eq. (7) simplifies to

$$m_p = m_p(0) \tag{13}$$

Since the particle mass m_p and diameter d_p do not change in this case, the particle density ρ_p also remains constant. If $\rho_p = \rho_{p0}$ is known, Eqs. (1)–(8) can be integrated to determine the particle trajectory ($x_p(t)$ and $y_p(t)$). If ρ_p is not known, it can be iteratively adjusted until the trajectory fits the mean measured particle positions ($\overline{x}_{p,i}$ and $\overline{y}_{p,i}$). Such a procedure allows for determining ρ_p by solving the following weighted least squares problem

$$\min_{\rho_p} \sum_{i=1}^{N} w_i[(x_{p,i}(\rho_p)-\overline{x}_{p,i})^2 + (y_{p,i}(\rho_p)-\overline{y}_{p,i})^2] \tag{14}$$

where N is the number of discrete mean trajectory positions (feeder positions) and w_i are weights calculated as

$$w_i = \frac{n_i}{n_t} N \tag{15}$$

where n_i is the number of recorded particles in single feeder position i and n_t is the total number of recorded particles (from all the feeder positions). The number of recorded particles in each observation window n_i is different, therefore the weights represent the contribution of each feeder position to the objective function (14). The sum of the weights is therefore equal to the number feeder positions.

3.2.2. The reactive case

If the particle is reactive, the mean reaction rate constant R_c can be determined in the same way as the particle density ρ_p in the non-reactive case. In the reactive case however, the initial particle density ρ_{p0}

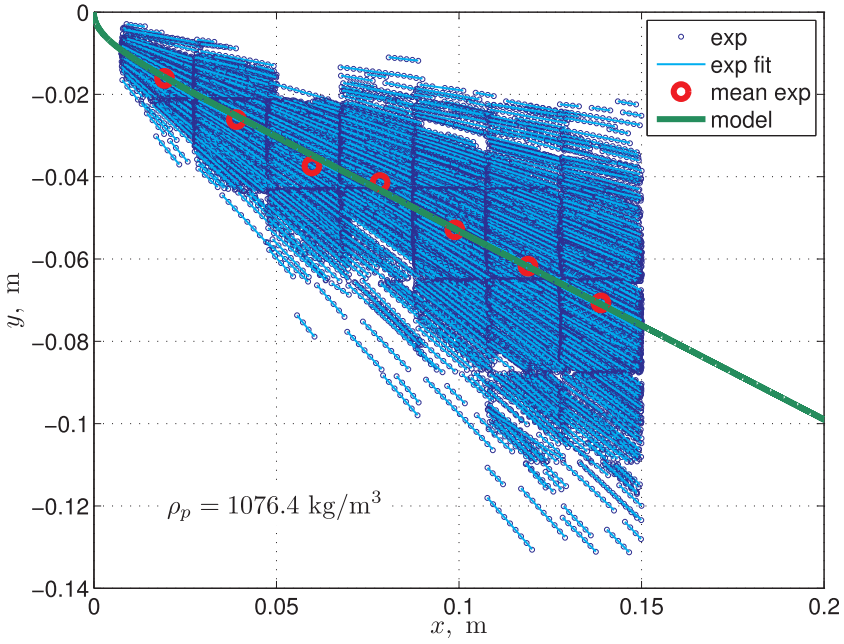

Fig. 9. Measured particle positions (exp), linear fit of the positions (exp fit), mean particle position in each observation window (mean exp) and fitted mean particle trajectory obtained from the inverse method (model).

must be known and it is determined from the non-reactive case. In order to find the mean reaction rate R_c, the following minimization problem is then solved

$$\min_{R_c} \sum_{i=1}^{N} w_i[(x_{p,i}(R_c)-\overline{x}_{p,i})^2 + (y_{p,i}(R_c)-\overline{y}_{p,i})^2] \quad (16)$$

3.2.3. Numerical solution

The sets of ordinary differential equations for non-reactive and reactive cases are solved using the explicit Runge–Kutta (4,5) method and the minimization problem is solved using the Pattern Search solver, both implemented in MATLAB [27].

4. Results and discussion

4.1. The non-reactive case

As mentioned earlier the material density of the particles can be determined by conducting non-reactive experiments. The non-reactive experiment was conducted for the Janina coal char. The char was milled and sieved to obtain a narrow particle size distribution. The experiment was conducted in nitrogen at 1000 °C. The mass flow rate of the carrier nitrogen was 0.224 gs^{-1}. The resulting measured particle positions are presented in Fig. 9. The positions were then approximated by a linear function (exp fit) and a mean particle position was computed in each observation window (mean exp). As can be observed, the non-reacting particles follow straight lines and the particles form an expanding cloud of trajectories. The reason for the large spread of the particles positions are the natural in–homogeneous properties of individual particles, which include diameter, shape, ash content, etc. Although the particles were sieved before the experiment with a sieve mesh size difference of 5 μm the size distribution is much wider (cf. Fig. 7) due to the longitudinal shape of some fraction of the particles and inaccuracy of the optical measurement. All these factors influence the broadening of the cloud.

The mean positions (mean exp) presented in Fig. 9 were then used in the inverse analysis to find the particle density ρ_p. The data required to perform the inverse analysis are presented in Table 3. The table contains also the standard deviations of the data, which will be used in the forthcoming section for sensitivity analysis and uncertainty quantification. The standard deviations were not required for the current calculations. The particle material density obtained from the inverse analysis is $\rho_p = 1076.4\ \mathrm{kg\ m^{-3}}$. The corresponding mean particle trajectory (model) is presented in Fig. 9 as well. Initially, the modeled particle falls into the chamber with initial vertical velocity component $v_p(0) = -v_t$ and passes the boundary layer (cf. Fig. 6) virtually without any horizontal displacement. As it becomes exposed to higher gas velocities, its horizontal velocity component v_p becomes larger up to a point where the forces acting on the particle equilibrate and the particle starts to follow a straight line. This is due to the fact that the particle mass does not change, and the gas velocity is virtually constant, outside the boundary layer. As can be seen, the fitted trajectory follows the experimentally determined mean particle positions and thus, it is representative for all the particles. The determined particle material density was then used as the initial density in the reactive experiments.

4.2. The reactive cases

Three experiments of coal char combustion in air were conducted. The same Janina coal char (collected from the same sample) as in the non-reactive case was used. The experiments differed by the oxidizer and chamber temperatures. The three temperatures were 850 °C, 950 °C and 1050 °C. The burning particles were recorded and their positions were used to determine the mean particle positions in each observation window. These positions were then used in the inverse analysis in which the mean reaction rate constant R_c was determined by fitting the modeled reactive particle trajectory to the mean positions. In Table 5 the data used in the calculations are presented. The presented standard deviations will be used in the forthcoming section for sensitivity analysis and uncertainty quantification and were not required at this stage. The recorded trajectories, their mean positions in the observation windows and the resulting modeled particle trajectory obtained from the inverse analysis, are presented in Fig. 10. As can be seen, the measured particle positions are very scattered, however the mean particle positions in each observation window (mean exp) follow an expected pattern, i.e. a visible non-linear shape of the first six points may be observed, which corresponds to intensive combustion of particle. Then a transition to more linear shape of the remaining points occurs, which corresponds to the place of final burnout of the particles. After that regions the particles, composed of ash, are not burning, and move along straight lines. There were 7392 particles recorded in this experiment and thus, each of the mean positions were determined

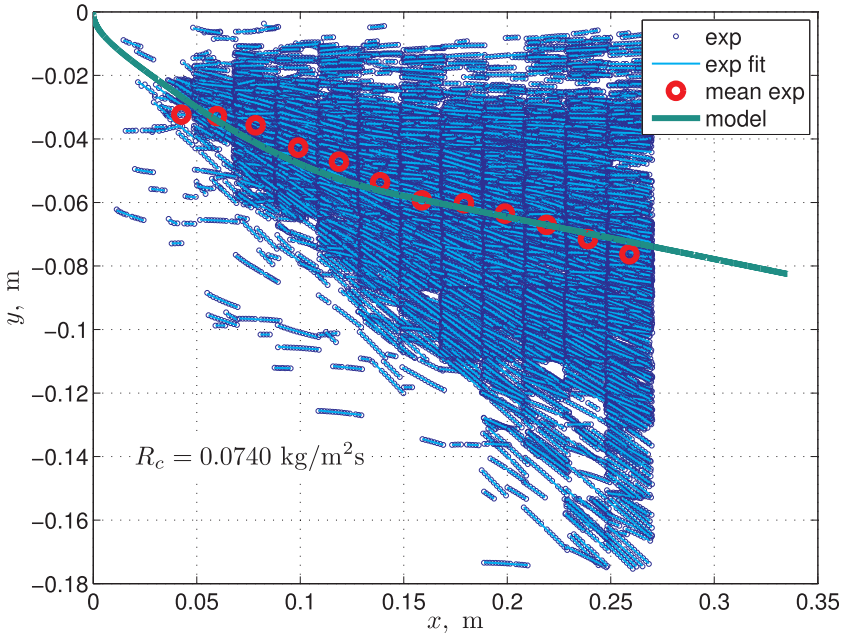

Fig. 10. Measured particle positions (exp), linear fit of the positions (exp fit), mean particle position in each observation window (mean exp) and fitted mean particle trajectory obtained from the inverse method (model).

based on a large number of recorded particles. The same behavior as for the mean particle positions can be observed for the modeled particle trajectory. The particle enters the test chamber while, due to the reaction, its mass changes, which is the reason for the curved trajectory. When all the carbon present in the particle is consumed, the particle composed of only ash moves along a straight line. The determined mean reaction rate constant for this experiment was $R_c = 0.0740$ kg m^{-2} s^{-1}. The particle diameter varies during combustion. In this study it was assumed that the variation in particle diameter is linear in time while varying from the initial to the final diameter. The initial diameter is the mean measured diameter in the non-reactive case, while the final diameter was selected to be the mean measured diameter for the reactive case from the last observation window, which corresponds to the end of combustion.

The variation of particle mass, which is a dependent variable in the equation set, as well as the variation of particle diameter, affect the particle density. The calculated changes of particle mass, diameter and density in the course of combustion are presented in Fig. 11.

In Table 4 the retrieved mean reaction rate constant for all three experiments is presented. As expected, an increasing mean reaction rate constant with increasing temperature is observed.

4.3. Sensitivity analysis and uncertainty quantification

The developed model for retrieving the mean particle density and mean reaction rate requires using input data, which are measured and are subject to uncertainty. The uncertainty propagates through the model and affects the uncertainty of the model output. It is therefore important to quantify this uncertainty. A global sensitivity analysis (SA) and uncertainty quantification (UQ) was performed to examine the influence of each of the input parameters on the obtained results and to quantify the resulting uncertainty of the model output. The analysis was realized using the Dakota [28] software. Latin hypercube sampling (LHS) was used, which allows to sample the parameter space effectively. The task was divided into two parts. In the first part, the non-reactive case was examined in which the key input parameter (d_p) was identified and the uncertainty of the particle density was determined. The resulting probability distribution of the particle density was then used in the second part, where the uncertainty of the mean reaction rate constant was determined for the experiments with the three different temperatures discussed earlier. The uncertainties were assumed to be aleatory and were determined for each of the measured parameters. Five input parameters (d_p,v_t,ϕ,$\dot{m}$ and T) were considered for the non-reactive case. The uncertainties for d_p,v_t and ϕ were determined from the measurements, while for $\dot{m}$ and T they were obtained from calibration certificates of the measurement devices. The parameters along with their mean values for this case were presented in Table 3. For the reactive cases, the set was extended by the particle density ρ_p. For this case, the data were presented in Table 5, except the last column, where the particle density is shown. For the SA and UQ study for the reactive case the probability distribution function of particle density obtained from the non-reactive case was used to characterize the distribution. All the input parameters, besides the particle density, were assumed to be normally distributed. For the particle diameter d_p and particle inlet velocity v_p this assumption was verified by examination of normal quantile plots. One can see from Figs. 7 and 8, that their distributions virtually follow the normal distribution. It should be stressed here that the uncertainties in determination of the mean particle positions in both the non-reactive case and the reactive cases are ignored. This will lead to an underestimated final uncertainty. The parameter space was sampled with 17500 runs of the model in the non-reactive case. Further examination of the convergence of model output statistics revealed that 10 000 samples for the reactive case is sufficient and thus, this number of samples was used for all the reactive cases.

In Fig. 12 the variation of the particle density with the individual parameters are presented along with a liner fit indicating the linear mutual dependence of the variables. As can be seen, the strongest and

Table 4
Retrieved mean reaction rate constants R_c.

T (°C)	850	950	1050
R_c (kg m^{-2}s^{-1}	0.025	0.074	0.089

Table 5
Mean values μ and standard deviations σ of the parameters in the three experiments in air.

Experiment		d_p (μm)	v_t (m s^{-1})	ϕ (−)	$\dot{m}$ (g s^{-1})	T (K)	ρ_p (kg m^{-3})
1	μ	119.2	0.1808	0.7737	0.261222	1123.15	1076.4
	σ	15.9	0.0361	0.0580	0.000522	1.57	–
2	μ	119.2	0.1727	0.7737	0.239861	1223.15	1076.4
	σ	15.9	0.0345	0.0580	0.000480	1.72	–
3	μ	119.2	0.1654	0.7737	0.221750	1323.15	1076.4
	σ	15.9	0.0331	0.0580	0.000443	1.87	–

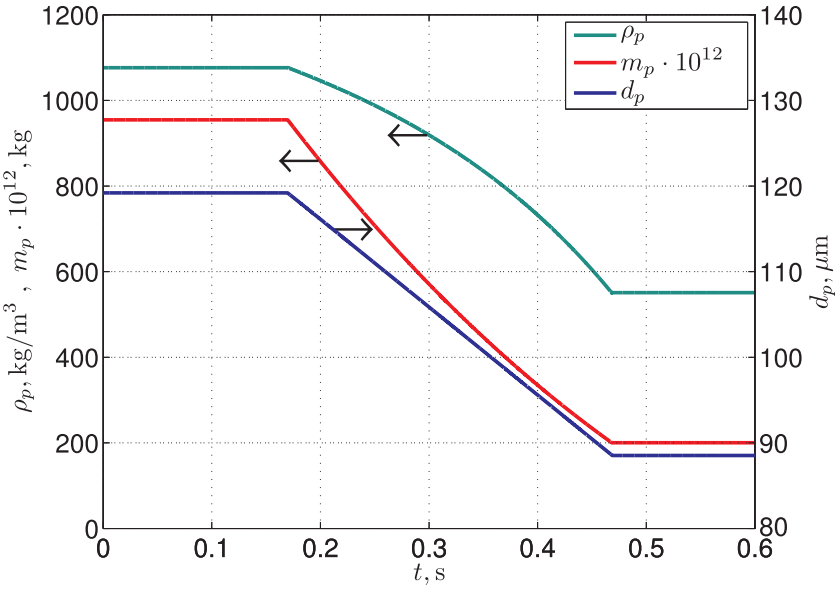

Fig. 11. Variation of particle mass, diameter and density during combustion.

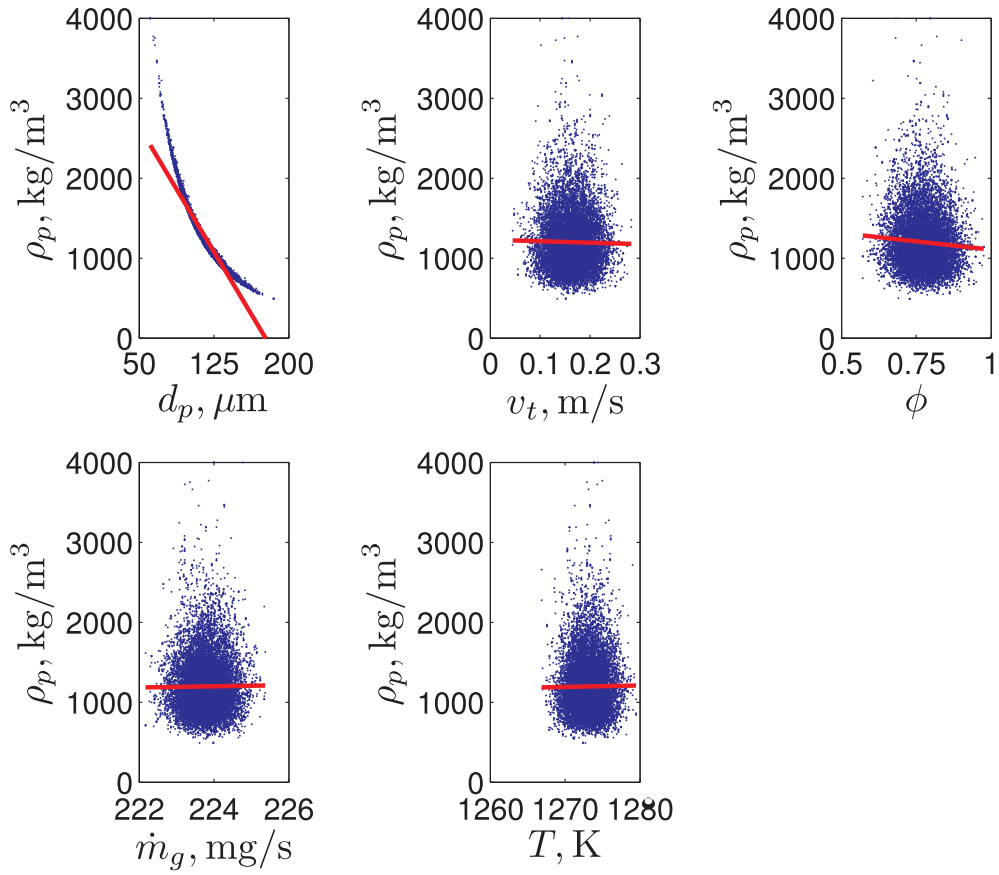

Fig. 12. Variation of the model output (particle density) for subsequent model input parameters.

non-linear dependence is observed for the the particle diameter. The remaining parameters exhibit weak influence on the output. This can be confirmed by investigation of the partial correlation coefficients presented in Fig. 13. As suspected the key input parameter is the particle diameter, which has the strongest influence on the model output. Much smaller influence can be observed for the particle sphericity. The correlation coefficients for both parameters are negative, indicating a decrease of the model output ρ_p with increasing d_p and ϕ. The three remaining model inputs are of minor importance. This is due to both small influence of these parameters on the particle density determination and their relatively small uncertainties. In Fig. 14, the resultant probability density function (PDF) and cumulative distribution function

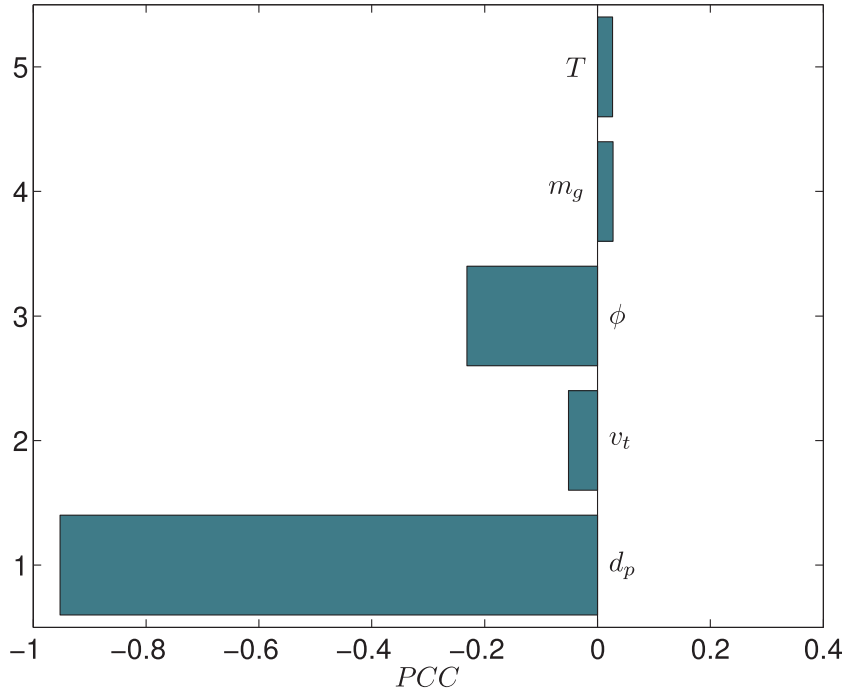

Fig. 13. Partial correlation coefficients for the individual input parameters in the non-reactive case.

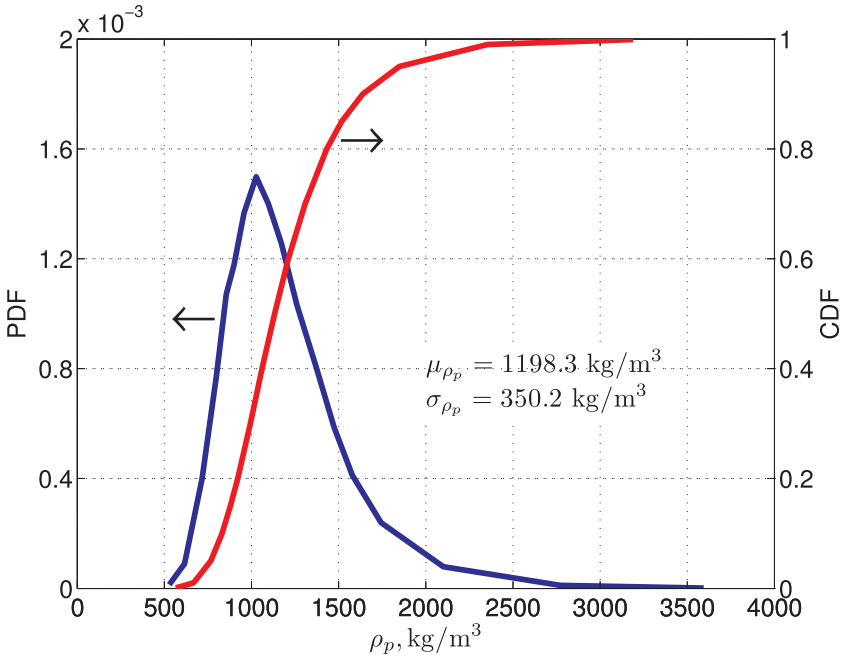

Fig. 14. Probability density function and cumulative distribution of the particle density.

(CDF) of the particle density ρ_p are presented. As can be observed, the distribution is skewed and the standard deviation is very large, indicating strong variation of the particle density with the changes of the input parameters, from which the most important is the particle diameter. The obtained mean particle material density of 1198.3 kg m^{-3}, is very close to the values obtained by Bibrzycki et al. [29] for the same coal, where for char obtained with a low heating rate the density was 1257 kg m^{-3} and for char obtained with higher heating rate it was 1163 kg m^{-3}.

The distribution of particle density presented in Fig. 14 was then used as the input in the analysis of reactive cases.

Similarly to the analysis presented for particle material density, the SA and UQ were performed for the mean reaction rate constant R_c. As mentioned earlier the input parameters for the reactive cases were summarized in Table 5 except for the particle density, whose PDF was taken from the non-reactive case. Furthermore, since the correlation among the parameters from the non-reactive case were known at this stage, they were used in the reactive case study, so that the mutual dependencies were taken into account [28,30].

In Fig. 15, the partial correlation coefficients of the input variables for the experiment at $T = 850$ °C are presented. As can be seen, the strongest dependence on the model output R_c can be attributed to particle diameter and particle density. Some influence of the particle sphericity is also visible, however it is much smaller. The remaining parameters do not exhibit any influence on the output. It can therefore be concluded that the uncertainty quantification could be performed for the two (d_p,ρ_p) or three (including ϕ) main inputs only and omitting the remaining parameters. The statistics are however computed from the

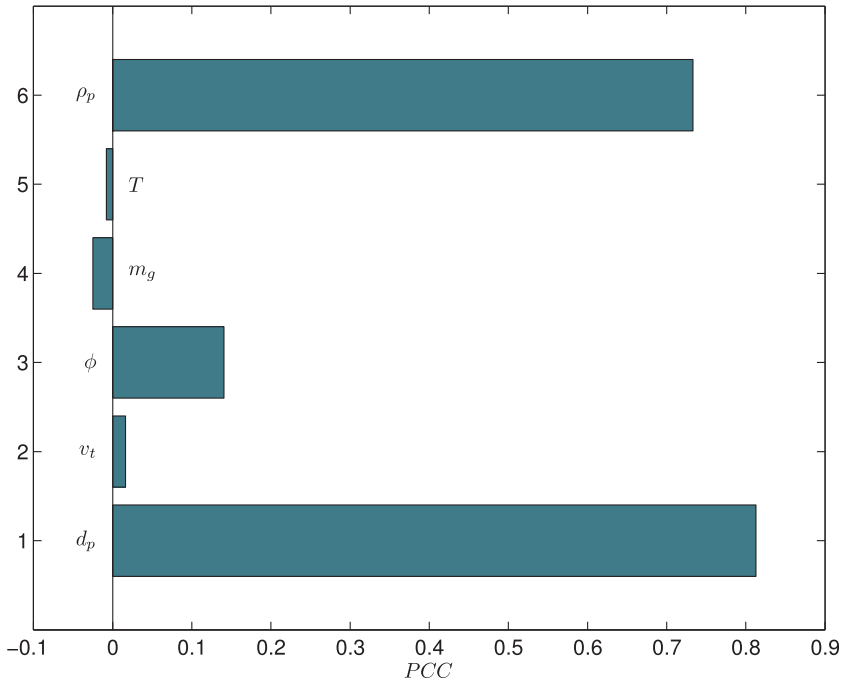

Fig. 15. Partial correlation coefficients for the individual input parameters in the reactive case.

same sample set and thus the unimportant parameters were also included. In Figs. 16–18 the obtained PDFs and CDFs are presented along with the corresponding means and standard deviations for the three examined temperatures. As can be seen, the distributions range from negative values of R_c to as high positive values as 0.5. The negative values of R_c are nonphysical and correspond to a situation where the particle mass is increasing in the reactor. This is however possible in the computational procedure due to the fact that the parameters are drawn from their distributions and a selected set of input data may be unfavorable in the sens that only a negative R_c may fit the experimental data. In Fig. 19 the obtained mean reaction rate constants and their standard deviations (the height of the error bars correspond to two standard deviations) are presented. As can be noticed, the mean reaction rate constants are growing with increasing temperatures which is in accordance with intuition and with the result obtained without uncertainty quantification (cf. Table 4). As expected, the results obtained without uncertainty quantification, for a single run of the model with mean input parameters, are different from the mean values obtained with UQ. The obtained standard deviations are large and the reason of that are the uncertainties in particle diameter and particle density measurement. Since the uncertainties in determination of the mean particle positions in both the non-reactive case and the reactive cases were ignored it can be concluded that the final uncertainties are still underestimated. An increased resolution of the camera could reduce the uncertainty, which would improve the particle diameter and sphericity measurement accuracy. A more accurate method of determination of particle density could also reduce the uncertainty.

5. Validation of the results

When a new experimental and/or computational method is introduced, it is important to evaluate its credibility. For the Janina coal examined within this study, experimental data of char combustion in air was available [29]. This data was obtained using TGA, which is known to produce satisfactory results in the kinetic regime, i.e. at low temperatures (lower than ~ 950 K) due to the diffusion restrictions at higher temperatures. Experimental results presented in [29] were obtained using TGA for two chars at various temperatures ranging from 623 K to 1223 K. The two chars were generated at two different heating rates; char 1 at 590 K/min and char 2 at 10 K/min. In the study the intrinsic reactivity was also determined, however for the comparison with LFDF only the mean conversion rates were used.

The three experiments of char combustion in air using the LFDF and presented in the previous sections of this study were compared with the experimental data in [29].

For completeness of the comparison the diffusion restriction for a single particle at the conditions and particle size of the LFDF was also calculated to present the limit of the reaction rate at high temperatures. By assuming diffusion controlled reactions, i.e. that the reaction rate is controlled entirely by the diffusive transport of oxygen to the particle surface, and by assuming that the oxygen reacts with carbon to produce CO2 (not CO) such that equimolar counterdiffusion is maintained [31], the specific char conversion rate is given by

$$\Theta = -\frac{1}{m_{p0}}\frac{dm_p}{dt} = \frac{1}{m_{p0}}\frac{M_C}{M_{O_2}}\mathrm{Sh}D\pi d_p\rho_{O_2} \tag{17}$$

where M_C and M_{O_2} are molecular weights of carbon and oxygen, Sh is the Sherwood number, D is the binary diffusion coefficient, d_p is the particle diameter and m_{p0} is the initial particle mass. The binary diffusion coefficient was calculated for O_2 - *air* pair using the Chapman-Enskog kinetic theory [32]. The Sherwood number was calculated from [33].

$$\mathrm{Sh} = 2.0 + 0.6\mathrm{Re}_p^{0.5}\mathrm{Sc}^{0.33} \tag{18}$$

where Sc is the Schmidt number defined as

$$\mathrm{Sc} = \frac{\nu}{D} \tag{19}$$

The properties of the fluid required to calculate the conversion rate were determined at the bulk fluid conditions [29]. The Reynolds number was calculated for the initial particle diameter $d_{p0} = 119.2\,\mu\mathrm{m}$, and velocity equal to the terminal fall velocity of a particle with material density of $\rho_{p0} = 1198.3\,\mathrm{kg\,m^{-3}}$, as measured in the LFDF experiment in nitrogen. In Fig. 20 the conversion rates determined from the LFDF experiment and from the TGA [29] for both chars are presented. The diffusion controlled reaction obtained from Eq. (17) for a single particle combustion, which limits the reaction rate at high temperatures, is also presented. The mean conversion rate due to chemical reaction at low temperatures for char 1 is shown as a dotted line. As will be discussed in next section, char 1 conversion rate was used to determine kinetic-diffusion model parameters, thus this line was created only for char 1. The mean diffusion restriction for both chars obtained

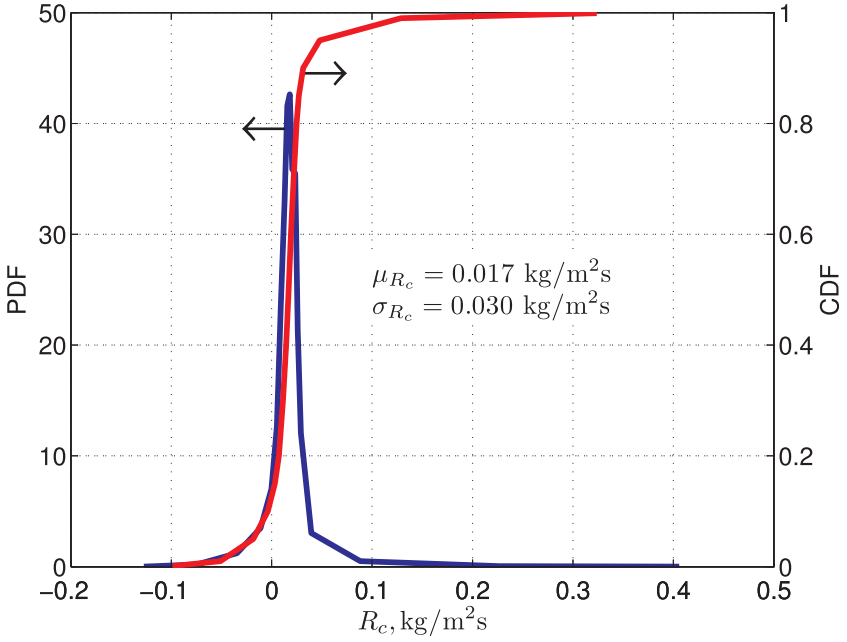

Fig. 16. Probability density function and cumulative distribution of the mean reaction rate constant at 850 °C.

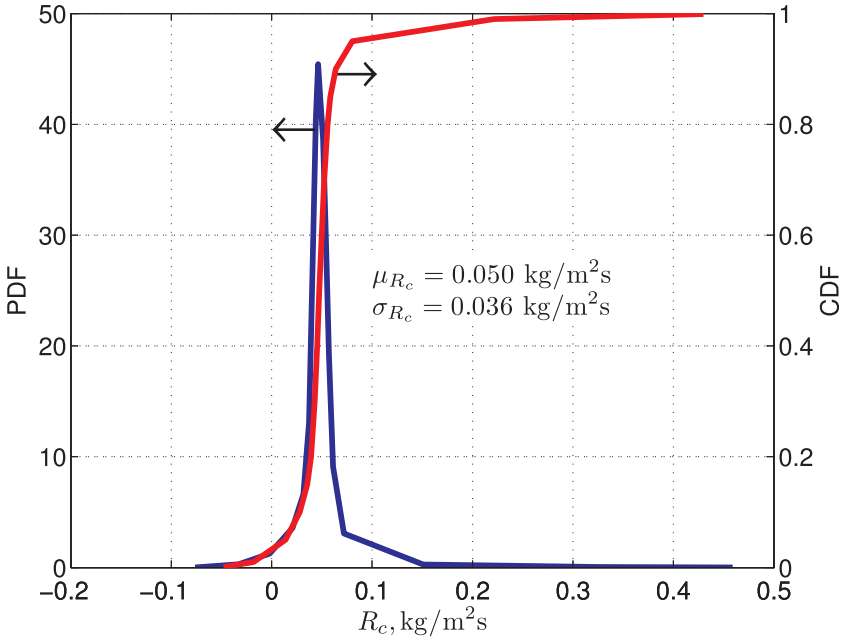

Fig. 17. Probability density function and cumulative distribution of the mean reaction rate constant at 950 °C.

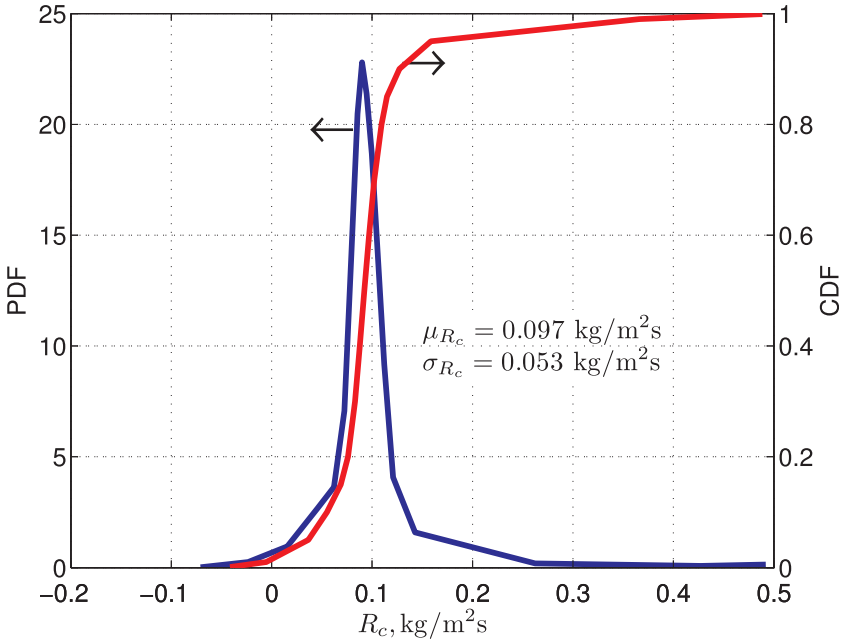

Fig. 18. Probability density function and cumulative distribution of the mean reaction rate constant at 1050 °C.

by approximating the TGA data at high temperatures is also presented. The convergence of the TGA data at high temperatures confirms that the process is independent of char type and diffusion limited. As can be seen, the predicted conversion rates from the LFDF experiments fit in the allowable region of the plot. As expected at low temperatures the data tend to the chemical reaction line whereas the diffusion restriction for single particle is approached at high temperatures. The results are presented with uncertainties (standard deviations), however for the lowest temperature (T = 850 °C) the mean minus the standard deviation ($\mu-\sigma$) is not visible on the log scale plot since the value is negative (cf. Fig. 19).

6. Kinetic-diffusion model

In this section a kinetic-diffusion surface combustion model is fitted to the experimental data. The data used are the mean reaction rates obtained from TGA for char 1 and from the LFDF presented in Fig. 20. The data for char 1 was selected due to the fact that it was produced with a higher heating rate, which is closer to conditions in real combustion chambers than the heating rate used to produce char 2. The kinetic diffusion model of Baum and Street [34] and Field [35] was used, which is a standard model in several CFD solvers, and allows a direct use of the measured kinetics in further CFD models. The model has the following form

$$\frac{dm_p}{dt} = -A_p p_{O_2} \frac{1}{1/R_{dif} + 1/R_{kin}} \tag{20}$$

where A_p is the particle external surface area, p_{O_2} is the partial pressure of oxygen in air. R_{dif} is the reaction rate due to diffusion

$$R_{dif} = \frac{C}{d_p}\left(\frac{T + T_p}{2}\right)^{0.75} \tag{21}$$

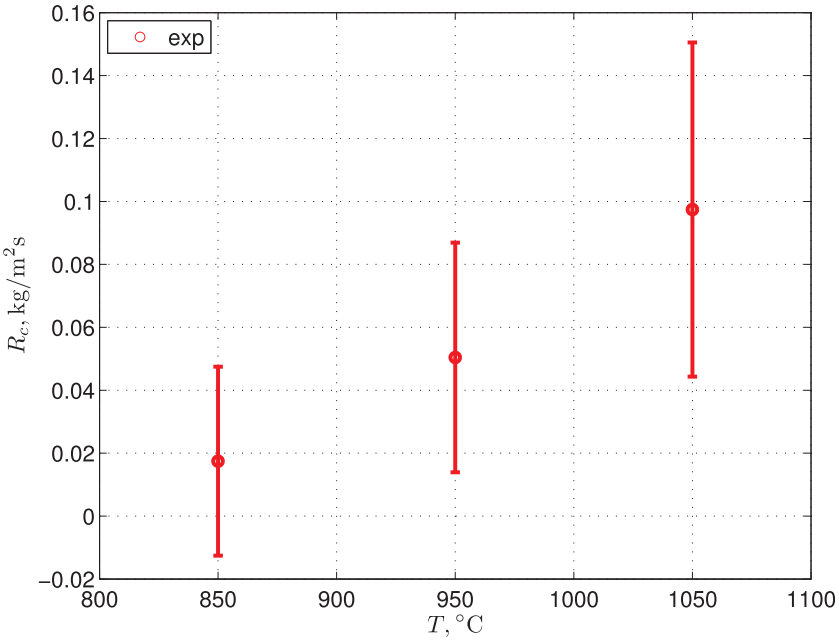

Fig. 19. Comparison of the obtained mean reaction rate constants and their standard deviations. The error bar height equals two standard deviations.

and R_{kin} is the kinetic rate

$$R_{kin} = A\exp\left(-\frac{E}{RT_p}\right) \tag{22}$$

where d_p is the particle diameter, T_p and T are the temperatures of the particle and of the gas surrounding the particle, respectively, R is the universal gas constant and C,A and E are model constants. Since the particle temperature was not measured in the experiments, it was assumed that the temperatures T and T_p are equal. As discussed in Section 3.1.1, the particle surface temperatures can be a few hundred Kelvins higher than the gas temperature, thus this assumption may lead to errors. It should be also stressed that only the three first TGA data points corresponding to the lowest temperatures were used in the fitting procedure. This is due to the fact that the four remaining points correspond to the too low reaction rate due to diffusion restrictions in the TGA. The fitted kinetic-diffusion model is presented in Fig. 20. The obtained model constants are $C = 1.823 \times 10^{12}$s K$^{-0.75}$,$A = 1.435$ s m^{-1} and $E = 1.245 \times 10^{8}$J kmol^{-1} and can be used for CFD simulations of the Janina coal combustion in air.

7. Conclusions

A new method for retrieving solid fuel conversion rates has been presented. Experiments conducted in nitrogen and air at various temperatures allowed the mean particle density and rate constant to be determined. Global sensitivity analysis and uncertainty quantification were then conducted to determine the key parameters affecting the results and to quantify uncertainty in the computed particle density and mean reaction rate constants. The uncertainties in determination of the mean particle positions in both the non-reactive case and the reactive cases were ignored leading to underestimated final uncertainties. The sensitivity analysis indicated that the most important parameter is the

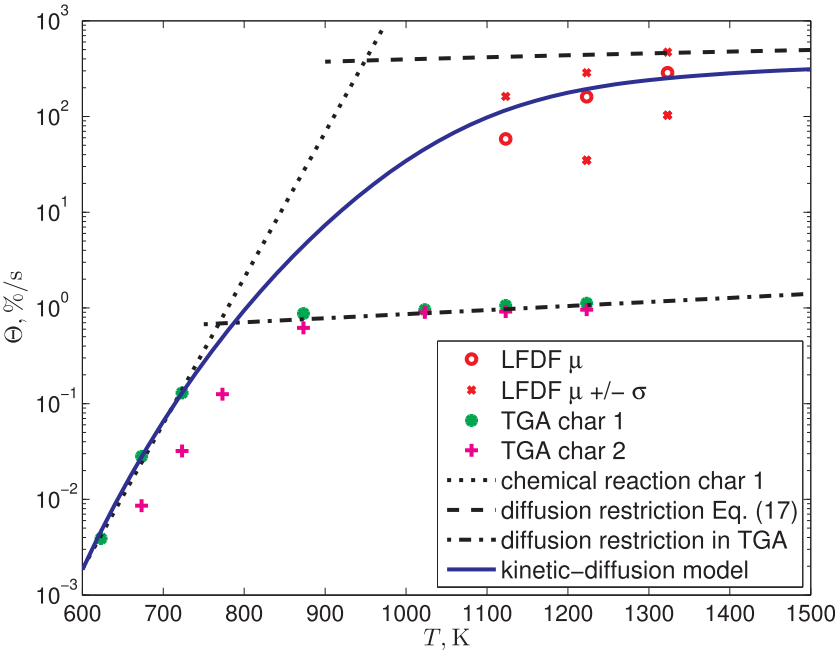

Fig. 20. Comparison of the mean conversion rates determined using the LFDF and TGA [29] and the fitted kinetic-diffusion model.

particle diameter, which affects the determined particle density and further the mean rate constant. The quantified uncertainties of the results are relatively large and could be reduced by more accurate measurements of particle diameters. This could be done by using a higher resolution camera in the test rig. The results obtained with the presented method were then compared with results obtained from the literature (TGA) for the same coal and atmosphere. The comparison indicated that appropriate trends were obtained: the data approach the chemical reaction limit at low temperatures and the diffusion limit at high temperatures. Due to lack of other results, the method could not be compared with other methods at exactly the same conditions. Finally, coefficients of a kinetic-diffusion surface reaction model were determined by fitting the model to the TGA and LFDF data.

The developed methodology is appropriate and suitable to determine the kinetic data, however it has to be further developed in order to improve the accuracy of the measurements and include the more complex physico-chemical processes that occur in reality during carbon conversion. In particular a better camera should be used to reduce the uncertainties of diameter and sphericity measurements. Furthermore particle temperatures should be measured and incorporated in the model.

Acknowledgments

The research leading to these results has received funding from the Polish-Norwegian Research Program operated by the National Center for Research and Development under the Norwegian Financial Mechanism 2009–2014 in the frame of Project Contract No Pol-Nor/232738/101/2014.

References

[1] Biagini E, Tognotti L. A generalized correlation for coal devolatilization kinetics at high temperature. Fuel Process Technol 2014;126:513–20. http://dx.doi.org/10.1016/j.fuproc.2014.06.008. http://www.sciencedirect.com/science/article/pii/S0378382014002458.

[2] Authier O, Thunin E, Plion P, Schonnenbeck C, Leyssens G, Brilhac J-F, et al. Kinetic study of pulverized coal devolatilization for boiler CFD modeling. Fuel 2014;122:254–60. http://dx.doi.org/10.1016/j.fuel.2014.01.026. http://www.sciencedirect.com/science/article/pii/S0016236114000362.

[3] Zhang DK, Wall TF. Coal utilization and the environment ignition of coal particles: the influence of experimental technique. Fuel 1994;73(7):1114–9. http://dx.doi.org/10.1016/0016-2361(94)90247-X.

[4] Wall TF, Gupta RP, Gururajan VS, Zhang DK. The ignition of coal particles. Fuel 1991;70(9):1011–6. http://dx.doi.org/10.1016/0016-2361(91)90252-6.

[5] Essenhigh RH, Misra MK, Shaw DW. Ignition of coal particles: a review. Combust Flame 1989;77(1):3–30. http://dx.doi.org/10.1016/0010-2180(89)90101-6.

[6] Khatami R, Stivers C, Levendis YA. Ignition characteristics of single coal particles from three different ranks in O2/N2 and O2/CO2 atmospheres. Combust Flame 2012;159(12):3554–68. http://dx.doi.org/10.1016/j.combustflame.2012.06.019. http://www.sciencedirect.com/science/article/pii/S001021801200199X.

[7] Shaddix CR, Molina A. Particle imaging of ignition and devolatilization of pulverized coal during oxy-fuel combustion. Proc Combust Inst 2009;32(2):2091–8. http://dx.doi.org/10.1016/j.proci.2008.06.157. http://www.sciencedirect.com/science/article/pii/S1540748908002770.

[8] Septien S, Valin S, Dupont C, Peyrot M, Salvador S. Effect of particle size and temperature on woody biomass fast pyrolysis at high temperature (1000–1400c). Fuel 2012;97:202–10. http://dx.doi.org/10.1016/j.fuel.2012.01.049. http://www.sciencedirect.com/science/article/pii/S0016236112000919.

[9] Jones J, Patterson P, Pourkashanian M, Williams A, Arenillas A, Rubiera F, et al. Modelling NOx formation in coal particle combustion at high temperature: an investigation of the devolatilisation kinetic factors. Fuel 1999;78(10):1171–9. http://dx.doi.org/10.1016/S0016-2361(99)00024-1. http://www.sciencedirect.com/science/article/pii/S0016236199000241.

[10] Wang G, Zander R, Costa M. Oxy-fuel combustion characteristics of pulverized-coal in a drop tube furnace. Fuel 2014;115:452–60. http://dx.doi.org/10.1016/j.fuel.2013.07.063.

[11] Bejarano PA, Levendis YA. Single-coal-particle combustion in O2/N2 and O2/CO2 environments. Combust Flame 2008;153(1–2):270–87. http://dx.doi.org/10.1016/j.combustflame.2007.10.022. http://www.sciencedirect.com/science/article/pii/S0010218007003276.

[12] Rathnam RK, Elliott LK, Wall TF, Liu Y, Moghtaderi B. Differences in reactivity of pulverised coal in air (O2/N2) and oxy-fuel (O2/CO2) conditions. Fuel Process Technol 2009;90(6):797–802. http://dx.doi.org/10.1016/j.fuproc.2009.02.009. http://www.sciencedirect.com/science/article/pii/S0378382009000411.

[13] Zhang L, Binner E, Qiao Y, Li C-Z. In situ diagnostics of victorian brown coal combustion in O2/N2 and O2/CO2 mixtures in drop-tube furnace. Fuel 2010;89(10):2703–12. http://dx.doi.org/10.1016/j.fuel.2010.04.020. http://www.sciencedirect.com/science/article/pii/S0016236110001936.

[14] Wang Y, Bell DA. Reaction kinetics of powder river basin coal gasification in carbon dioxide using a modified drop tube reactor. Fuel 2015;140:616–25. http://dx.doi.org/10.1016/j.fuel.2014.09.106. http://www.sciencedirect.com/science/article/pii/S0016236114009752.

[15] Umemoto S, Kajitani S, Hara S. Modeling of coal char gasification in coexistence of CO2 and H2O considering sharing of active sites. Fuel 2013;103:14–21. http://dx.doi.org/10.1016/j.fuel.2011.11.030.

[16] Kajitani S, Hara S, Matsuda H. Gasification rate analysis of coal char with a pressurized drop tube furnace. Fuel 2002;81(5):539–46. http://dx.doi.org/10.1016/S0016-2361(01)00149-1.

[17] Harris D, Roberts D, Henderson D. Gasification behaviour of australian coals at high temperature and pressure, Fuel 85(2), 2006, pp. 134–142, In: special Issue: The 21st Annual International Pittsburgh Coal Conference. doi: 10.1016/j.fuel.2005.07.022. http://www.sciencedirect.com/science/article/pii/S0016236105002917.

[18] Schulze S, Nikrityuk P, Abosteif Z, Guhl S, Richter A, Meyer B. Heat and mass transfer within thermogravimetric analyser: from simulation to improved estimation of kinetic data for char gasification. Fuel 2017;187:338–48. http://dx.doi.org/10.1016/j.fuel.2016.09.048. http://www.sciencedirect.com/science/article/pii/S001623611630905X.

[19] Adamczyk WP, Szlek A, Klimanek A, Bialecki RA, Wecel G, Katelbach-Wozniak A, et al. Visualization system for the measurement of size and sphericity of char particles under combustion conditions. Powder Technol. 2016;301:141–52. http://dx.doi.org/10.1016/j.powtec.2016.06.004. http://www.sciencedirect.com/science/article/pii/S0032591016303321.

[20] Adamczyk WP, Szlęk A, Klimanek A, Białecki RA, Węcel G, Katelbach-Woźniak A, et al. Design of the experimental rig for retrieving kinetic data of char particles. Fuel Process Technol 2017;156:178–84. http://dx.doi.org/10.1016/j.fuproc.2016.10.031.

[21] Fox RW, McDonald AT. Introduction to Fluid Mechanics. 5th Ed. New Delhi, India: John Wiley & Sons Inc; 2004.

[22] Haider A, Levenspiel O. Drag coefficient and terminal velocity of spherical and nonspherical particles. Powder Technol 1989;58:63–70.

[23] Richter A, Nikrityuk PA, Meyer B. Three-dimensional calculation of a chemically reacting porous particle moving in a hot O2/CO2 atmosphere. Int J Heat Mass Transf 2015;83:244–58. http://dx.doi.org/10.1016/j.ijheatmasstransfer.2014.11.090. http://linkinghub.elsevier.com/retrieve/pii/S0017931014010904.

[24] Murphy JJ, Shaddix CR. Combustion kinetics of coal chars in oxygen-enriched environments. Combust Flame 2006;144(4):710–29. http://dx.doi.org/10.1016/j.combustflame.2005.08.039. http://www.sciencedirect.com/science/article/pii/S0010218005002658.

[25] Spiga M, Morino G. A symmetric solution for velocity profile in laminar flow through rectangular ducts. Int Commun Heat Mass Transf 1994;21(4):469–75. http://dx.doi.org/10.1016/0735-1933(94)90046-9. http://www.scopus.com/inward/record.url?eid=2-s2.0-0028468927 & partnerID=tZOtx3y1.

[26] Blythman R, Jeffers N, Persoons T, Murray D. Localized and Time-Resolved Velocity Measurements of Pulsatile Flow in a Rectangular Channel. Int J Mech Aerosp Ind Mech Manuf Eng 2016;10(2):469–75. scholar.waset.org/1999.8/10003482.

[27] MATLAB, 7.9.0.529 (R2009b), The MathWorks Inc., Natick, Massachusetts, 2009.

[28] Adams B, Bauman L, Bohnhoff W, Dalbey K, Ebeida M, Eddy J, et al. A Multilevel Parallel Object-Oriented Framework for Design Optimization, Parameter Estimation, Uncertainty Quantification, and Sensitivity Analysis: Version 6.4 User's Manual, updated May 2016 Edition, Sandia Technical Report SAND2014-4633, 2014.

[29] Bibrzycki J, Mancini M, Szlek A, Weber R. A char combustion sub-model for cfd-predictions of fluidized bed combustion - experiments and mathematical modeling. Combust Flame 2016;163:188–201. http://dx.doi.org/10.1016/j.combustflame.2015.09.024. http://www.sciencedirect.com/science/article/pii/S0010218015003272.

[30] Iman R, Conover W. A distribution-free approach to inducing rank correlation among input variables. Commun Stat Simulat Comput 1982;B11(3):311–34.

[31] Hayhurst AN. The mass transfer coefficient for oxygen reacting with a carbon particle in a fluidized or packed bed. Combust Flame 2000;121:679–88.

[32] Bird R, Stewart W, Lightfoot E. Transport Phenomena. 2nd Ed. Wiley-india; 2006.

[33] Ranz W, Marshall WR. Evaporation from Drops, Part I. Chem Eng Prog 1952;48(3):141–6.

[34] Baum MM, Street PJ. Predicting the combustion behaviour of coal particles. Combust Sci Technol 1971;3(5):231–43. http://dx.doi.org/10.1080/00102207108952290.

[35] Field M. Rate of combustion of size-graded fractions of char from a low-rank coal between 1. Combust Flame 1969;13(3):237–52. http://dx.doi.org/10.1016/0010-2180(69)90002-9.